Multibond Dynamics of Nanoscale Friction: The Role of Temperature

Itay Barel and Michael Urbakh
School of Chemistry, Tel Aviv University, 69978 Tel Aviv, Israel

Lars Jansen and André Schirmeisen*
Institute of Physics and Center for Nanotechnology (CeNTech), University of Münster, Münster, Germany
(Received 15 October 2009; published 12 February 2010)

The main challenge in predicting sliding friction is related to the complexity of highly nonequilibrium processes, the kinetics of which are controlled by the interface temperature. Our experiments reveal a nonmonotonic enhancement of dry nanoscale friction at cryogenic temperatures for different material classes. Concerted simulations show that it emerges from two competing processes acting at the interface: the thermally activated formation as well as rupturing of an ensemble of atomic contacts. These results provide a new conceptual framework to describe the dynamics of dry friction.

DOI: 10.1103/PhysRevLett.104.066104 PACS numbers: 68.35.Af, 07.79.Sp, 46.55.+d

Despite the practical and fundamental importance of friction in completely different fields from the nanometer contacts inherent in micro- and nanomachines [1] and biological molecular motors [2] to the geophysical scales characteristic for earthquakes [3], many key aspects of the dynamics of friction are still not well understood. One of the main difficulties in understanding and predicting frictional response is the complexity of highly nonequilibrium processes going on in any tribological contact which include detachment and reattachment of multiple microscopic junctions (bonds) between the surfaces in relative motion [1–7]. If these detachment and reattachment processes are thermally activated, temperature must play an important role for the kinetics of friction. But what is the resulting temperature dependence of friction? The energy landscape of two surfaces in contact exhibits a lot of metastable states, and thermal excitations can provide sufficient energy to overcome local barriers and enable slip. Thus, a general prediction is that interfacial friction should decrease with temperature provided no other surface or material parameters are altered by the temperature changes [8–13]. Here we demonstrate the breakdown of this simple prediction in nanoscale friction experiments and report that the friction force exhibits a peak at cryogenic temperatures for different classes of materials, including amorphous, crystalline, and layered surfaces. We propose a model that reproduces the experimental observations by explicitly considering the influence of temperature on the formation and rupturing of microscopic contacts.

Experiments of nanoscopic friction under controlled vacuum conditions over a wide temperature range have reported a strong increase of friction on graphite and MoS_2 below 300 K [14,15], crossing over to temperature independent friction below a threshold of 220 K. This finding was linked to the onset of wear processes [15]. Measurements of point contact friction in the wearless regime from room temperature down to 50 K were reported for a nanoscopic silicon contact [16]. In this case, evidence for strongly nonlinear friction-temperature behavior was provided, including a strong enhancement of friction around 100 K. Recent simulations performed within the Prandtl-Tomlinson model have revealed that the temperature can affect the slip length resulting in a rich temperature dependence of friction [17], but some model assumptions were strongly idealized not representing the experimental conditions in [14–16].

Here, we performed nanoscale friction experiments under clean ultrahigh vacuum conditions with an atomic force microscope as a function of sample temperature at cryogenic temperatures from 30 K to room temperature. In order to avoid ambiguities, the same type of cantilever was used in all experiments. The cantilever is fabricated from Si(111); however, the sliding tip apex is covered with an amorphous silicon oxide layer. We used cantilevers with a low normal force spring constants of 0.05 N/m and applying tip loads below 50 nN, which yielded no measurable surface wear during scanning. Furthermore, we measured the pull-off force at all temperatures, allowing us to monitor strong changes of the tip-sample adhesion, which would indicate significant alterations of the tip geometry.

Sample materials were chosen to represent a wide range of different material properties, including amorphous and crystalline surfaces. First, a Si(111) wafer with an amorphous silicon oxide surface was chosen, thus consistent with the tip apex material. The second sample was a SiC wafer, heated in vacuum to remove contaminations from air. As examples for crystalline surfaces, we investigated an air cleaved and annealed ionic crystal [NaCl(001)] and a vacuum cleaved layered semimetal (highly oriented pyrolytic graphite—HOPG). On those two samples, friction was measured on atomically flat terraces [18].

The results of the average friction force as a function of sample temperature ranging from 30 to 300 K are shown in Figure. 1 for the four samples. Despite the wide range of sample properties, all friction curves show similar characteristic temperature dependencies. Initially we find a dis-

tinct friction enhancement when decreasing the temperature from ambient to low temperatures. Most prominently, a further reduction of temperature leads to decrease of friction again resulting in a friction peak at different temperatures ranging from 55 ± 10 K for Si, 120 ± 15 K for SiC, 110 ± 20 K for NaCl, and 100 ± 25 K for HOPG. In contrast to the friction data, the simultaneously measured adhesion temperature curves show no strong features or systematic behavior.

In order to mimic the AFM measurements in our simulations, we consider a rigid tip with mass M and center-of-mass coordinate X that interacts with the underlying surface through an array of contacts representing the molecular bonds, as depicted in Fig. 2 [18]. Recent simulations have revealed that even for an apparently smooth but amorphous carbon tip apex sliding on a crystalline diamond surface [19], the interface consists of an ensemble of individual atomic contacts. Thus we envision the amorphous silicon oxide tip sliding on the various hard surfaces to also consist of randomly distributed molecular bonds which, in first approximation, behave as independent individual contacts. Although the exact nature of the bonds is unknown at this point, we expect weak bond energies due to the inertness of silicon oxide, with only little dependence on the chemical nature of the surface.

The tip is pulled along the surface with a constant velocity V through a linear spring of spring constant K. We model the contacts (N of them) by elastic springs, each with a force constant κ and a rest length $l^{(0)}$. As long as a contact is unbroken, it is stretched in the lateral direction while a ruptured contact relaxes rapidly to its equilibrium state. We consider rupture of contacts as a thermally assisted escape from a bound state over an activation barrier $\Delta E_{\mathrm{off}}(f_i)$, which is force dependent and diminishes as the applied elastic force, f_i, increases [6,20]. Precisely this mechanism characterizes the Prandtl-Tomlinson type models, which have been surprisingly successful in describing atomic scale friction phenomena until now [8,9,13,21].

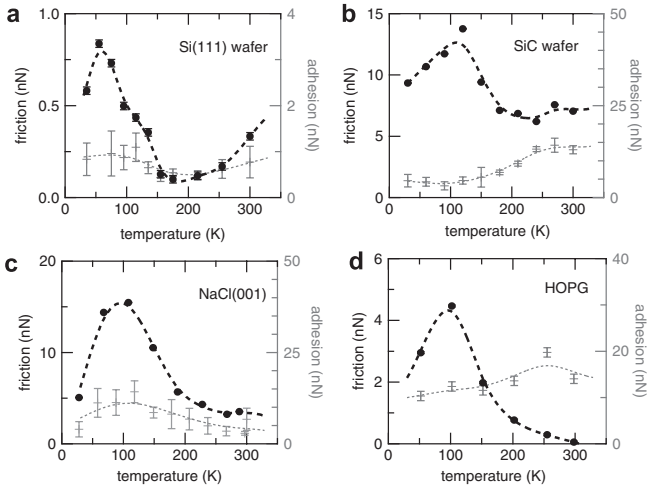

FIG. 1. Friction (solid black markers, left-hand scale) and corresponding adhesion values (grey crosses, right-hand scale) measured in ultrahigh vacuum with a silicon cantilever as a function of temperature for four different sample surfaces. (a) Si(111) wafer, (b) SiC wafer, (c) atomically flat terraces on a cleaved NaCl(001) crystal, and (d) a HOPG surface. The externally applied normal loads were $F_{\mathrm{load}} = 1.6$, 15, 53, and 1.7 nN for the Si, SiC, NaCl, and HOPG samples, respectively.

What has rarely been rationalized so far is that a second process must be considered as well [6]: the formation of individual contacts, characterized by a further energy barrier ΔE_{on} which is needed to initiate the contact. Contact formation as well as contact rupturing processes are thermally activated, and we expect a complex interdependence of bonding and rupturing with tip velocity and temperature. In the Prandtl-Tomlinson model the distance traversed by the tip during sliding is determined by periodicity of the surface potential. Here it is defined by the interplay between the rupture and reattachment rates.

For moderate or high potential barriers (the barrier height $\Delta E_{\mathrm{off}} \gg k_B T$), the rupture occurs preferentially when the contact is close to its slippage condition, and the rate, $k_{\mathrm{off}}(f_i)$, can be approximated by [6,20]:

$$k_{\mathrm{off}}(f_i) = \omega^0_{\mathrm{off}} \exp[-\Delta E_{\mathrm{off}}(1 - f_i/f_c)^{3/2}/k_B T]. \quad (1)$$

Here ω^0_{off} and ΔE_{off} are the characteristic attempt frequency and the height of potential barrier for unbinding in the absence of the external force, respectively, and f_c is the critical force at which the potential barrier, $\Delta E_{\mathrm{off}}(f_i)$, vanishes. The formation of contacts is described by the rate

$$k_{\mathrm{on}} = \omega^0_{\mathrm{on}} \exp[-\Delta E_{\mathrm{on}}/k_B T],$$

where ω^0_{on} and ΔE_{on} are the attempting frequency and the barrier height for the reattachment. The stochastic nature of both rupture and reattachment processes is included in our simulations.

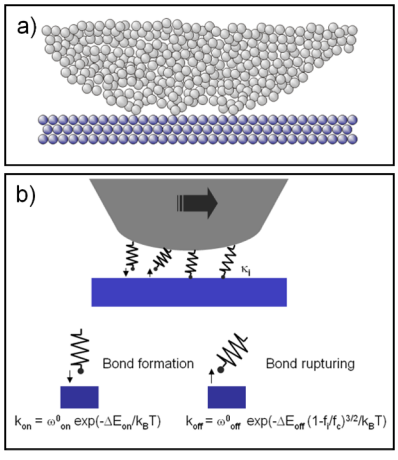

FIG. 2 (color online). (a) Sketch of a typical geometry for an amorphous tip sliding on a flat crystalline surface. (b) Model to simulate multiple contacts at the tip-sample interface. Rates of contact formation and rupturing processes are determined by the heights of the corresponding energy barriers, ΔE_{on} and ΔE_{off}.

In our model, the dynamics of friction is determined by four characteristic frequencies (rates): the rate of spontaneous detachment of contacts, $k^0_{\rm off} = k_{\rm off}(f_i = 0)$, the rate of contact formation, $k_{\rm on}$, the rate of forced unbinding, KV/f_s, and a characteristic rate of the pulling force relaxation, $\omega_m = \max(K/\eta, \sqrt{K/M})$, where η is a damping coefficient responsible for the dissipation of the tip kinetic energy. The rates, $k^0_{\rm off}$ and $k_{\rm on}$, are defined by inherent microscopic properties of the system, and they depend on temperature, while the rates KV/f_c and ω_m are temperature independent and influenced by the pulling velocity V and mechanical parameters of the experimental setup, M and K.

Figure 3(a) shows the temperature dependence of the time-averaged spring force, $\langle F \rangle$, calculated for a number of pulling velocities. We find the same characteristic friction enhancement peak at low temperatures as observed in the experiments. For the tip velocities considered here, the temperature of the peak is changing systematically, shifting to higher values for increasing tip velocity. The simulation parameters were adjusted to fit the friction-temperature curves for the silicon sample, since those experiments were performed with the highest density of data points on the temperature axis. However, the overall behavior is found for a large variety of simulation parameters, as long as the activation energies for rupture and reattachment lie in the range of $\Delta E_{\rm off} \approx 0.10$–$0.25$ eV, $\Delta E_{\rm on} \approx 0.05$–$0.15$ eV and the number of contacts is not less than 20, which are realistic assumptions for the experiments (see, e.g., Ref. [19]). It should be noted that the characteristic features of our experimental results (the peak in friction at cryogenic temperatures, the magnitude of friction force at the maximum that is of the order of 1 nN, and the steep decrease of friction above the peak temperature) cannot be reproduced by a model that includes only one or few contacts, which is the central assumption of Tomlinson-like models.

Figure 3(b) shows the experimental friction-temperature curves from the silicon sample for direct comparison. For this sample, we measured friction also as a function of scan speed, ranging from 250 nm/s to 16100 nm/s. The friction peak shifts by roughly $\Delta T = 20$ K to higher values with increasing scan speed. A direct fingerprint of the peak shift with velocity is found in Fig. 3(d), which shows the experimental velocity dependence of friction at constant temperatures, $T = 35$ K, $T = 75$ K, and $T = 135$ K. At temperatures above the peak temperature, friction increases with scan speed, whereas at a temperature below the peak temperature, friction decreases with velocity. A decrease of friction with velocity has been also observed in recent AFM experiments [22] correlated to rupture and reformation of molecular bonds. Our simulations provide a direct link between the temperature and velocity dependencies of friction, and they show the experimentally observed fingerprint in the friction-velocity curves in Fig. 3(c). Apparently, the model captures the essential

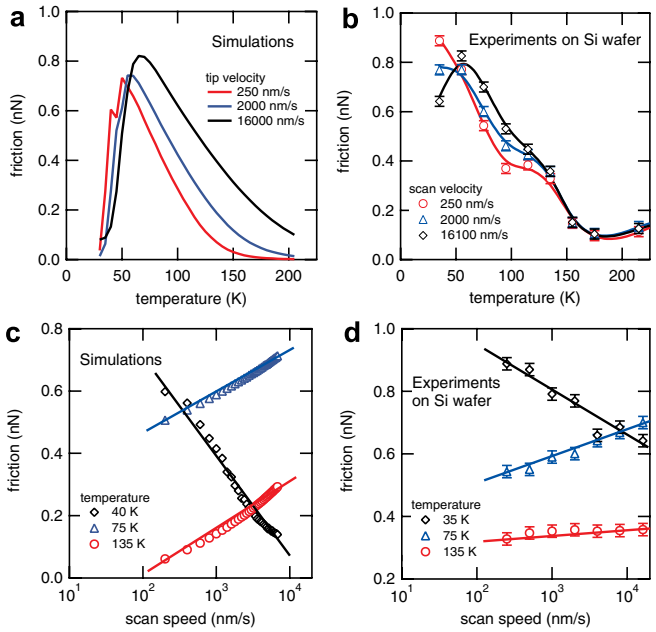

FIG. 3 (color online). Comparison of friction simulations and experiments. (a) Simulated time-averaged friction as a function of temperature for different sliding speeds. (b) Experimental friction-temperature curves on the silicon sample for the same scan velocities. (c) Simulated friction-velocity curves for the different temperatures showing characteristic negative and positive slopes. (d) Experimental friction as a function of scan velocity for the same temperatures. Parameter values used in simulations: $\omega^0_{\rm off} = \omega^0_{\rm on} = 10^{10}$ s^{-1}, $\Delta E_{\rm off} = 0.15$ eV, $\Delta E_{\rm on} = 0.05$ eV, $\kappa = 1$ N/m, $f_c = 0.16$ nN, $N = 20$, $\eta = 5 \times 10^{-6}$ kg/s, $K = 6$ N/m, and $M = 5 \times 10^{-11}$ kg.

elements necessary to describe the friction-temperature and friction-velocity behavior of nanoscale contacts.

In order to elucidate the origin of the observed temperature behavior we present in Fig. 4 time series of the spring force which were calculated for five characteristic temperatures. At low temperatures when the rate of contact formation is smaller than a characteristic rate of forced unbinding, $k_{\rm on} < KV/f_c$, only few contacts can be formed simultaneously during sliding. Then the mean friction force can be estimated as [18]

$$\langle F \rangle = (f_c^2 \omega^0_{\rm on}/2KV) \exp[-\Delta E_{\rm on}/k_B T]. \qquad (3)$$

With increase of temperature, the rate of reattachment, $k_{\rm on}$, rises that leads to an increase of a number of simultaneously attached contacts and to an enhancement of the mean friction force. Accordingly, the force traces, $F(t)$, start to exhibit a typical stick-slip behavior that keeps on up to the temperatures for which $k_{\rm on} \approx \omega_m$ [Figs. 4(b) and 4(c)]. In this regime, the stick-slip motion is characterized by a cooperative behavior of contacts. As the reattachment rate, $k_{\rm on}$, approaches the rate of force relaxation, ω_m, the stick-slip motion becomes more and more irregular, and for $k_{\rm on} > \omega_m$ the force traces become completely erratic [see Fig. 4(d)]. The mean friction force $\langle F \rangle$

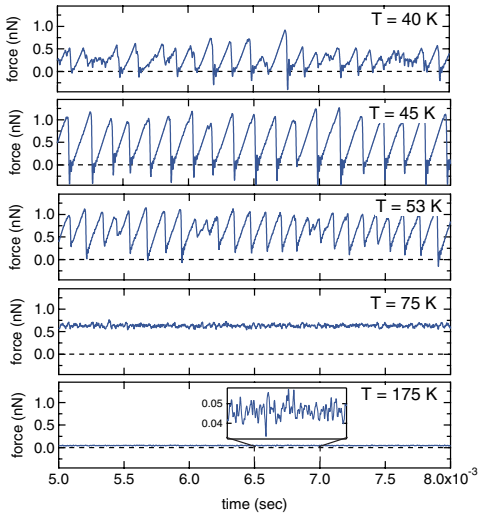

FIG. 4 (color online). Representative parts of time series of the simulated friction forces at different temperatures. The friction versus time curves show a transition from periodic sequential stick-slip behavior at low temperatures to the stochastic behavior of simultaneous multiple bonds formation and breaking processes at higher temperatures (tip velocity $V = 2000$ nm/s, other parameter, as in Fig. 3).

as a function of T peaks at the temperature $T_{\max}$ for which $k_{\text{on}} \approx \omega_m$.

Immediately above the maximum at $T = T_{\max}$, the decrease of friction with T is determined by the effect of thermally induced reduction of the contact rupture forces. In this case, the mean force can be written as [6]:

$$\langle F \rangle \approx N f_c \left\{ 1 - \left(\frac{k_B T}{\Delta E_{\text{off}}} \right)^{2/3} \left[\ln \left(\frac{3 \Delta E_{\text{off}} K V}{2 k_B T \omega_{\text{off}}^0 f_c N^2} \right) \right]^{2/3} \right\}. \tag{4}$$

At higher temperatures (i.e., where $k_{\text{off}}^0 > KV/f_c$), the rupture of contacts is determined by the rate of spontaneous unbinding k_{off}^0. Then the kinetic frictional force can be estimated taking into account that a contact elongates on average by a length $\approx V/k_{\text{off}}^0$ when in the intact state, and

$$\langle F \rangle \approx \kappa V N \langle \nu_{\text{int}} \rangle \exp(\Delta E_{\text{off}}/k_B T)/\omega_{\text{off}}^0, \tag{5}$$

where $\langle \nu_{\text{int}} \rangle$ is a time-averaged fraction of the intact contacts that is close to its equilibrium value, $k_{\text{on}}/(k_{\text{on}} + k_{\text{off}}^0)$.

Equations (3) and (5) predict an exponential dependence of friction on $1/T$ in both low and high temperature limits, $\langle F \rangle \propto \exp(-\Delta E_{\text{on}}/k_B T)$ and $\langle F \rangle \propto \exp(\Delta E_{\text{off}}/k_B T)$, respectively. Thus, a treatment of experimental data obtained for low and high temperatures may allow extracting the activation energies for formation and rupture of atomic contacts, which are the key microscopic parameters of the system. For our experiments on the Si(111) wafer, we find that the activation energies for the contact rupture and reattachment equal to $\Delta E_{\text{off}} \approx 0.15$–$0.18$ eV and $\Delta E_{\text{on}} \approx 0.05$–$0.08$ eV. Exponential reduction of friction with T for high temperatures has been observed in recent experiments [14,15]. Please note that Eqs. (3) and (4) predict inverse dependencies of the friction force on the pulling velocity in low and high temperature regimes: a reduction of friction with velocity for low temperatures following $\langle F \rangle \propto 1/V$ and an increase of friction with velocity for high temperatures of the form $\langle F \rangle \propto \ln(V)^{2/3}$. Again, this is observed in both of our experiments and simulations [see Figs. 3(c) and 3(d)], thus solidifying the link between the observed complex temperature dependence of nanoscale friction with the dynamic behavior of an ensemble of microscopic contacts.

Discussions and support by H. Hölscher and H. Fuchs are gratefully acknowledged. The work in Tel Aviv, as part of the ESF EUROCORES Program FANAS (CRP ACOF), was supported by the Israel Science Foundation (1109/09) and the EC Sixth Framework Program ERASCT-2003-980409. Work in Münster was supported by the DFG (Grant No. SCHI 619/6-1).

*schirmeisen@uni-muenster.de

[1] M. Urbakh *et al.*, Nature (London) **430**, 525 (2004).
[2] V. Bormuth *et al.*, Science **325**, 870 (2009).
[3] C. H. Scholz, Nature (London) **391**, 37 (1998).
[4] R. Budakian and S. J. Putterman, Phys. Rev. Lett. **85**, 1000 (2000).
[5] E. Gerde and M. Marder, Nature (London) **413**, 285 (2001).
[6] A. E. Filippov, J. Klafter, and M. Urbakh, Phys. Rev. Lett. **92**, 135503 (2004).
[7] S. M. Rubinstein, G. Cohen, and J. Fineberg, Nature (London) **430**, 1005 (2004).
[8] Y. Sang, M. Dube, and M. Grant, Phys. Rev. Lett. **87**, 174301 (2001).
[9] O. Dudko *et al.*, Chem. Phys. Lett. **352**, 499 (2002).
[10] I. Szlufarska, M. Chandross, and R. W. Carpick, J. Phys. D **41**, 123001 (2008).
[11] W. K. Kim and M. L. Falk, Mater. Res. Soc. Symp. Proc. **1085**, 1085-T02-02 (2008).
[12] M. J. Brukman *et al.*, J. Phys. Chem. C **112**, 9358 (2008).
[13] P.Steiner *et al.*, Phys. Rev. B **79**, 045414 (2009).
[14] X. Zhao *et al.*, Tribol. Lett. **27**, 113 (2007).
[15] X. Zhao *et al.*, Phys. Rev. Lett. **102**, 186102 (2009).
[16] A. Schirmeisen *et al.*, Appl. Phys. Lett. **88**, 123108 (2006).
[17] Z. Tshiprut, S. Zelner, and M. Urbakh, Phys. Rev. Lett. **102**, 136102 (2009).
[18] See supplementary material at http://link.aps.org/supplemental/10.1103/PhysRevLett.104.066104 for experimental and simulation details.
[19] Y. Mo, K. T. Turner, and I. Szlufarska, Nature (London) **457**, 1116 (2009).
[20] O. K. Dudko *et al.*, Proc. Natl. Acad. Sci. U.S.A. **100**, 11 378 (2003).
[21] M. H. Muser, M. Urbakh, and M. O. Robbins, Adv. Chem. Phys. **126**, 187 (2003).
[22] J. Chen *et al.*, Phys. Rev. Lett. **96**, 236102 (2006).